

Reversible Inversion for Training-Free Exemplar-guided Image Editing

Yuke Li¹ Lianli Gao¹ Ji Zhang¹ Pengpeng Zeng² Lichuan Xiang³
 Hongkai Wen³ Heng Tao Shen² Jingkuan Song²

¹ University of Electronic Science and Technology of China ² Tongji University ³ University of Warwick



Figure 1. Exemplar-guided image editing results of our proposed *training-free* method **ReInversion**. The left column shows the source images, the three right columns show the generated results, each conditioned on a reference exemplar (denoted by a red border).

Abstract

Exemplar-guided Image Editing (EIE) aims to modify a source image according to a visual reference. Existing approaches often require large-scale pre-training to learn relationships between the source and reference images, incurring high computational costs. As a training-free alternative, inversion techniques can be used to map the source image into a latent space for manipulation. However, our empirical study reveals that standard inversion is sub-optimal for EIE, leading to poor quality and inefficiency. To tackle this challenge, we introduce **Reversible Inversion (ReInversion)** for effective and efficient EIE. Specifically, **ReInversion** operates as a two-stage denoising process, which is first conditioned on the source image and subsequently on the reference. Besides, we introduce a Mask-Guided Selective Denoising (MSD) strategy to constrain edits to target regions, preserving the structural consistency of the background. Both qualitative and quantitative comparisons

demonstrate that our **ReInversion** method achieves state-of-the-art EIE performance with the lowest computational overhead. Our code is available at [Code](#).

1. Introduction

Exemplar-guided image editing modifies a source image under the guidance of a reference exemplar, enabling precise control over visual attributes such as color, texture, or object appearance [3, 36, 39, 42, 43]. It provides fine-grained guidance that is difficult to express with language alone, allowing users to specify desired appearance directly through an example image. Consequently, exemplar-guided editing has emerged as a flexible and user-friendly paradigm for producing personalized and visually coherent results.

Despite substantial progress, existing EIE approaches typically require large-scale datasets to learn complex relational mappings between source and reference images. This process not only incurs significant computational costs dur-

ing training but also suffers from the scarcity of high-quality edited data pairs, since such pairs are difficult to obtain.

While training-free inversion methods [7, 9, 12, 23, 40] alleviate the need for large-scale training by mapping source images into a manipulable latent space that integrates reference information, they still face intrinsic limitations. Specifically, the backward inversion process cannot accurately recover previous latent states, relying instead on approximations from current predictions—leading to accumulated drift and degraded edit quality over time. Our experiments further confirm these issues, showing that directly applying standard inversion to EIE often results in inefficient and low-quality edits, as shown in Fig. 2 (b).

To overcome these limitations, we propose **Reversible Inversion (ReInversion)**, a novel and training-free framework designed for effective and efficient EIE. ReInversion reformulates the editing pipeline as a two-stage denoising process. This process is first conditioned on the source image to preserve its core content and structure, and only subsequently conditioned on the reference exemplar to inject the desired visual attributes. This strategic, sequential conditioning effectively mitigates the common failures of standard inversion. Furthermore, to address the practical need for localized edits, we introduce a *Mask-Guided Selective Denoising (MSD)* strategy. This module provides explicit spatial control, constraining ReInversion’s focus strictly to the target object regions defined by a mask. This ensures that while the target is faithfully edited, the structural consistency of the unrelated background is meticulously preserved. We conduct extensive qualitative and quantitative comparisons against other state-of-the-art methods. The results conclusively demonstrate that our ReInversion framework achieves the best EIE performance.

In summary, our contributions are as follows:

- To the best of our knowledge, this is the first work to apply inversion techniques for training-free exemplar-guided image editing (EIE).
- We present Reversible Inversion (ReInversion), a novel approach enabling effective and efficient EIE via a two-stage denoising process.
- Extensive experiments demonstrate that our ReInversion approach surpasses state-of-the-art methods in both EIE performance and computational efficiency.

2. Related Work

Exemplar-guided editing. Exemplar-guided Image Editing (EIE) modifies a source image under the guidance of reference exemplars, which can serve as an alternative or complement to textual instructions, enabling precise control over visual attributes. Paint-by-Example [43] integrates an exemplar image into a generative model and disentangles exemplar and source through information bottlenecks to

prevent trivial copying, enabling faithful local edits. Any-Door [3] extends this idea to object-level customization, allowing object transfer between images through identity and detail feature injection. PairEdit [21] formulates EIE as semantic variation learning between paired images, decoupling content preservation and semantic shift through dual LoRA adapters. Similar efforts, including REEDIT [32], ImageBrush [42] adopt reference exemplars as conditioning signals to achieve intuitive and semantically consistent EIE. Recent researches have focused on conditional image manipulation using various signals. Many methods condition generation on sketches, masks, depth maps, poses, or segmentation maps, enabling fine-grained control over visual attributes [2, 24, 45]. Besides, leveraging the power of large-scale pretrained Diffusion Transformers (DiT) [8, 27], in-context generation methods enable versatile, mask-free multi-condition image editing [4, 6, 37, 39]. Despite these advances, most EIE methods depend on large-scale pre-training, leading to high computational costs.

Inversion for editing. In image editing, the inversion technique is commonly used to map a real image back into its noise state, allowing modification through new textual prompts. Early works leverage pre-trained GANs [11, 14, 15] to invert real images into their latent space, enabling image reconstruction and semantic editing through latent manipulation [26, 38, 44, 46]. For diffusion models [13, 29, 30], existing inversion approaches aim to recover the noise trajectory of a given image, enabling faithful regeneration and downstream editing [22, 23, 25, 33]. More recently, flow-based and rectified flow (RF) models [1, 10, 18, 20] have been introduced as efficient alternatives, providing deterministic and nearly straight sampling trajectories by solving an ordinary differential equation (ODE) [16, 31]. RF-Inversion [28] employs an optimal-control formulation for faithful and editable inversion, while FTEDIT [41] introduces two-stage inversion with velocity refinement and invariance control to preserve contents, and FireFlow [7] propose faster and analytically stable inversion mechanisms for flow-based transformers. Though these inversion strategies can be applied to EIE, their inherently backward formulation often causes inversion drift and increased sampling time.

3. Preliminaries

3.1. Flow Matching

The objective of flow matching models is to parameterize an ordinary differential equation (ODE) that transports a prior distribution π_0 (e.g., Gaussian) to a data distribution π_1 :

$$dZ_t = v(Z_t, t)dt, \quad Z_0 \sim \pi_0, \quad t \in [0, 1], \quad (1)$$

where $v(Z_t, t)$ is a time varying velocity field, which can be parameterized by a neural network θ , and $t \in [0, 1]$ denotes

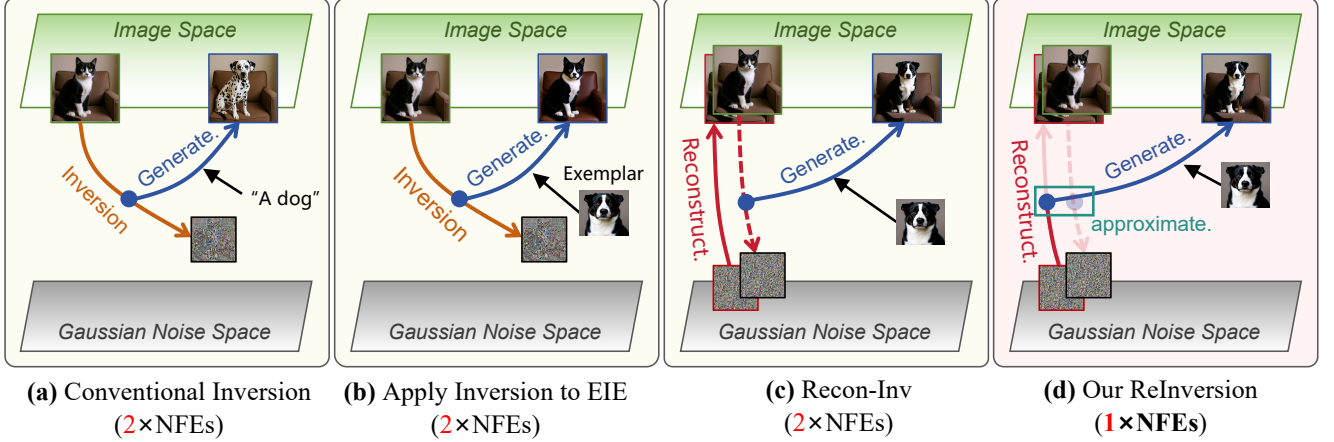


Figure 2. Comparison of inversion-based editing methods and our ReInversion. (a) Conventional inversion maps an source image to its approximate start noise and generates by a text guidance. (b) Inversion for EIE naively replaces the text condition with an exemplar, which leads to noise drift and undesirable edit result. (c) Reconstruction-Based Inversion (Recon-Inv) leverages the model’s forward reconstruction velocities to obtain a drift-free, reliable inversion from the source image. (d) Our ReInversion reformulates Recon-Inv into a $1 \times \text{NFEs}$ (Number of Function Evaluations) process and achieves faithful EIE.

the continuous time variable along the flow.

To solve this continuous ODE, a discrete numerical solver such as the Euler method can be applied. Using Euler solver, the integral can be discretized into n steps with timesteps $\{t_0, t_1, \dots, t_n\}$, where $t_0 = 0$ and $t_n = 1$. At each step t_i ($i \in \{0, \dots, n-1\}$), the network predicts $v_\theta(Z_{t_i}, t_i)$ and updates the state accordingly, resulting in $Z_1 \sim \pi_1$ after the final step. This iterative process can be formulated as:

$$Z_{t_{i+1}} = Z_{t_i} + (t_{i+1} - t_i) \cdot v_\theta(Z_{t_i}, t_i), \quad (2)$$

3.2. Inversion

Inversion-based editing aims to map a source image $X^s \sim \pi_1$ back to a near-noise state X_t (t is close to 0) while retaining its intrinsic content.

Derived from Eq. 2, the inversion from $X_{t_{i+1}}$ to X_{t_i} can be formulated as:

$$X_{t_i} = X_{t_{i+1}} - (t_{i+1} - t_i) \cdot v_\theta(X_{t_i}, t_i) \quad (3)$$

This ideal inversion is intractable in practice because the velocity field $v_\theta(X_{t_i}, t_i)$ depends on the unknown state X_{t_i} itself. A simple and common solution is to approximate $v_\theta(X_{t_i}, t_i)$ with $v_\theta(X_{t_{i+1}}, t_{i+1})$, that is:

$$X_{t_i} = X_{t_{i+1}} - (t_{i+1} - t_i) \cdot v_\theta(X_{t_{i+1}}, t_{i+1}). \quad (4)$$

This approximation introduces non-negligible error at each inversion step [9, 40]. As these errors accumulate over the backward trajectory, the estimated noise drifts from the prior distribution, leading to degraded editing performance, as illustrated in Fig. 2 (b).

The fundamental cause of this drift is the inaccessibility of the forward process during inversion: since the true forward trajectory and its velocity field $v_\theta(X_{t_i}, t_i)$ are unknown in the backward process, they must be estimated using the previous state $X_{t_{i+1}}$, which inevitably introduces errors. Existing methods have attempted to reduce this deviation using higher-order solvers [7, 34] or refined velocity estimation [9, 40, 41], but since they still rely on the backward trajectory, the fundamental limitation remains unresolved.

4. Method

To address the drift issue caused by the backward nature of conventional inversion, we first construct an explicit forward process, termed Reconstruction-Based Inversion, to ensure accurate reconstruction (Sec. 4.1). Then, we reformulate this process into our two-stage ReInversion that reduces sampling steps while maintaining editing fidelity (Sec. 4.2). Finally, we introduce a mask-guided selective denoising (MSD) module to enable localized and controllable edits (Sec. 4.3).

4.1. Reconstruction-Based Inversion

As detailed in Sec. 3.2, the forward process is typically inaccessible for conventional inversion-based editing, which often leads to the drift of estimated noise and consequently degrades editing fidelity. To address this issue, we construct an explicit forward process called Reconstruction-Based Inversion (Recon-Inv), enabling reliable velocity estimation at every timestep.

Specifically, this forward process is realized through the model’s reconstruction behavior. When only the source im-

age is provided without any editing instruction, the model takes $X^s \sim \pi_1$ as the sole condition and reconstructs it through its denoising process, preserving the original semantics.

Let \hat{X}_{t_i} denote the reconstruction state at timestep t_i and \hat{X}_1 the final reconstruction result. Starting from a sampled noise $X_0 \sim \pi_0$, the overall reconstruction process can be expressed as

$$\hat{X}_1 = X_0 + \sum_{i=0}^{n-1} (t_{i+1} - t_i) \cdot v_\theta(\hat{X}_{t_i}, t_i; X^s). \quad (5)$$

After obtaining the final reconstruction \hat{X}_1 , the corresponding velocity fields $v_\theta(\hat{X}_{t_i}, t_i; X^s)$ for all timesteps $i = 0, 1, \dots, n-1$ can be extracted from the reconstruction process for subsequent use. These velocities provide reliable and drift-free guidance across timesteps, allowing us to redefine the inversion as a forward-driven process.

Instead of estimating $v_\theta(X_{t_i}, t_i)$ as $v_\theta(X_{t_{i+1}}, t_{i+1})$ shown in Eq. 4, we directly use the velocities $v_\theta(\hat{X}_{t_i}, t_i)$ obtained during the forward reconstruction to define Recon-Inv, which is defined as

$$\tilde{X}_{t_i} = \tilde{X}_{t_{i+1}} - (t_{i+1} - t_i) \cdot v_\theta(\hat{X}_{t_i}, t_i; X^s), \quad (6)$$

where \tilde{X}_{t_i} denotes the inversion state at t_i and \tilde{X}_0 denotes the estimated noise of inversion. From the source image X^s , we can express Recon-Inv as:

$$\tilde{X}_0 = X^s - \sum_{i=0}^{n-1} (t_{i+1} - t_i) \cdot v_\theta(\hat{X}_{t_i}, t_i; X^s). \quad (7)$$

To understand the reliability of Recon-Inv, we analyze its error relative to the true initial noise X_0 . Combining Equations 5 and 7, we obtain

$$\underbrace{\|\tilde{X}_0 - X_0\|}_{\text{inv. error}} = \underbrace{\|X^s - \hat{X}_1\|}_{\text{recon. error}}, \quad (8)$$

where $\|a - b\|$ denotes the L_2 distance between image a and image b , which quantifies their discrepancy. In this equation, the inversion error on the left-hand side is exactly given by the reconstruction error on the right-hand side, linking the quality of the inversion to that of the reconstruction. Therefore, if the editing model θ achieves near-perfect reconstruction, i.e., $\|X^s - \hat{X}_1\| \rightarrow 0$, the Recon-Inv can achieve an errorless approximation of X^s .

To ensure accurate reconstruction and thus minimize the inversion error, we employ the recent pretrained editing model Flux-Kontext [17] that demonstrates strong reconstruction capability. As shown in Fig. 3, this model exhibits nearly perfect reconstruction ability. The reconstructed images are visually indistinguishable from the originals. In this way, we eliminate the need to approximate $v_\theta(X_{t_i}, t_i)$ from $v_\theta(X_{t_{i+1}}, t_{i+1})$, reducing noise drift and ensuring the following editing as shown in Fig. 2 (c).



Figure 3. Reconstruction results of Flux-Kontext [17]. Top: source images; bottom: reconstructions. The average per-pixel L_2 error is 0.016 on a $[0,1]$ scale.

4.2. Reversible Inversion

In Sec. 4.1, we introduced Recon-Inv, which provides a reliable inversion. However, this approach still requires nearly $2 \times$ NFEs (Number of Function Evaluations). In this subsection, we propose the two-stage Reversible Inversion (ReInversion), in order to achieve strong exemplar-guided editing with reduced sampling steps, illustrated in Fig 2 (d).

In the first stage of ReInversion, we reformulate Recon-Inv to obtain an intermediate transition state \tilde{X}_{t_τ} at timestep t_τ **directly from the source image X^s** , eliminating the need for a complete reconstruction process from noise to image. Introducing an intermediate transition state between the noisy and clean domains is a common practice in inversion [5, 19, 22]. This transition state preserves information from the source image X^s and serves as a starting point for subsequent exemplar-guided editing. Specifically, The transition state can be obtained by inverting from the source image X^s :

$$\tilde{X}_{t_\tau} = X^s - \sum_{i=\tau}^{n-\tau} (t_{i+1} - t_i) \cdot v_\theta(\hat{X}_{t_i}, t_i; X^s), \quad (9)$$

which, derived from Eq. 7, can be rewrite as

$$\tilde{X}_{t_\tau} = \tilde{X}_0 + \sum_{i=0}^{\tau-1} (t_{i+1} - t_i) \cdot v_\theta(\hat{X}_{t_i}, t_i; X^s). \quad (10)$$

According to Eq. 8 and Fig. 3, the difference between X_0 and \tilde{X}_0 is negligible. Hence, we can ignore their difference and reformulate the process as

$$\tilde{X}_{t_\tau} = X_0 + \sum_{i=0}^{\tau-1} (t_{i+1} - t_i) \cdot v_\theta(\tilde{X}_{t_i}, t_i; X^s). \quad (11)$$

This formulation corresponds to denoising from a gaussian noise X_0 to transition state guided by source image X^s , but without full reconstruction needed in Recon-Inv, thus eliminating redundant sampling steps. We further validate this reformulation through a quantitative comparison with Recon-Inv in Tab. 3.

In the second stage, we perform exemplar-guided editing starting from the transition state \tilde{X}_{t_τ} , where the reference condition X^r is incorporated to guide the editing process. We denote all the states of exemplar-guided editing as $X_{t_i}^{\text{edit}}$, where $t_i \in [0, 1]$, $X_0^{\text{edit}} = X_0 \sim \pi_0$, and X_1^{edit} represents the final edited result X^{edit} . Starting from the transition state $X_{t_\tau}^{\text{edit}}$, the editing process under the guidance of a reference image X^r .

$$X^{\text{edit}} = X_{t_\tau}^{\text{edit}} + \sum_{i=\tau}^{n-1} (t_{i+1} - t_i) \cdot v_\theta(X_{t_i}^{\text{edit}}, t_i; X^r) \quad (12)$$

Finally, the overall process of ReInversion from the noise state can be expressed as

$$X^{\text{edit}} = X_0^{\text{edit}} + \underbrace{\sum_{i=0}^{\tau-1} (t_{i+1} - t_i) \cdot v_\theta(X_{t_i}^{\text{edit}}, t_i; X^s)}_{\text{conditioned on } X^s} + \underbrace{\sum_{i=\tau}^{n-1} (t_{i+1} - t_i) \cdot v_\theta(X_{t_i}^{\text{edit}}, t_i; X^r)}_{\text{conditioned on } X^r}. \quad (13)$$

The proposed reformulation allows direct sampling from the prior noise distribution π_0 and conducting two-stage denoising. Alternatively, the velocity of the first stage $v_\theta(X_{t_i}^{\text{edit}}, t_i; X^s)$ can be replaced by a deterministic velocity $v^*(X_{t_i}^{\text{edit}}, t_i; X^s) = (X^s - X_{t_i}^{\text{edit}})/(1 - t_i)$. This velocity field directly points from the current state $X_{t_i}^{\text{edit}}$ toward X^s so that integrating it over time reconstructs X^s deterministically without relying on model prediction.

In summary, the first stage uses the source image X^s to preserve its structural details, while the second stage incorporates the reference X^r to transfer its desired attributes. This two-stage formulation achieves faithful and efficient exemplar-guided editing.

4.3. Mask-Guided Selective Denoising

In many editing scenarios, only a specific region of the source image needs to be modified while the surrounding background should remain unchanged. Yet, inversion-based methods lack explicit constraints on background preservation, often resulting in unwanted global alterations. Moreover, directly incorporating a user-provided mask without additional training is generally challenging.

To address this issue, we introduce Mask-Guided Selective Denoising (MSD) that enables spatially adaptive updates at the second stage of ReInversion. Given a binary mask $M \in \{0, 1\}^{H \times W \times 1}$, MSD can be formulated as

$$v_\theta^{\text{MSD}} = M \odot v_\theta + (1 - M) \odot (\eta \cdot v^* + (1 - \eta) \cdot v_\theta), \quad (14)$$

where \odot denotes element-wise multiplication, and we omit the explicit conditions of v_θ for brevity, which follow the

same definition in Eq. 11. $v^*(X_t^{\text{edit}}, t; X^s) = (X^s - X_t^{\text{edit}})/(1 - t)$ is a deterministic linear velocity field that transports the current latent state X_t toward the source image X^s . The scalar coefficient $\eta \in [0, 1]$ controls the strength of v^* outside the masked region, and we investigate its effect in Fig. 7.

The overall denoising trajectory from the transition state \tilde{X}_{t_τ} is then expressed as:

$$X^{\text{edit}} = \tilde{X}_{t_\tau} + \sum_{i=\tau}^{n-1} (t_{i+1} - t_i) v_\theta^{\text{MSD}}. \quad (15)$$

MSD allows the model to simultaneously denoise toward two targets under different spatial priors. In practice, the mask can be obtained from user input, automatic segmentation, or object detection, making the method flexible and generalizable to a wide range of editing tasks. Python-like pseudocode of our full method is provided in Supp. C.

5. Experiments

In this section, we first validate the effectiveness and efficiency of our ReInversion approach. Next, we present ablation studies to analyze the impacts of different factors on ReInversion. We start with an introduction of the experimental setup below.

5.1. Experimental Setup

Implementation Details. All experiments are conducted under a unified configuration on a single NVIDIA RTX A6000 GPU. We adopt Flux-Kontext-dev [17] as the backbone, with $n = 18$ denoising steps and no classifier-free guidance applied. The source, reference and generated images are all set to a resolution of 512×512 by default. Unless otherwise specified, we set the transition timestep to $t_\tau = 0.2$, indicating that during the denoising process the model follows the trajectory toward X^s before t_τ , and switches to be guided by X^r afterward. Since $n \cdot t_\tau \approx 4$, this corresponds to starting reference conditioning from the 4th step. This configuration ensures consistent and fair comparisons across all methods. More results on other backbones and steps is shown in Supp. B.

Evaluation Benchmark. We follow the common setup by evaluating our method on the COCOEE benchmark [43], which contains various exemplar-guided editing cases across real-world objects, including humans, animals, vehicles, and all kinds of common items. This dataset covers a wide range of scene layouts, providing a comprehensive testing benchmark for EIE. However, we observe that a notable portion of COCOEE samples suffer from low quality, where the reference exemplar is visually ambiguous or incomplete. For example, showing only a small part of the target object, containing severe distortions, or being heavily blurred. Such cases can lead to meaningless evaluations

Table 1. Quantitative comparison with state-of-the-art methods on COCOEE[†] benchmark. We comprehensively evaluate model performance from three aspects—Quality, Consistency and Efficiency. * denotes our approach using the deterministic velocity in stage-1.

Method	FID↓	QS↑	CLIP-FG↑	CLIP-BG↑	NFEs↓	Time Cost (s) ↓
Vanilla Inversion	33.76	21.24	71.42	60.77	56	20.89
RF-Inversion [28] (ICLR 2025)	9.09	64.17	77.94	66.50	56	23.37
FTEdit [41] (CVPR 2025)	23.81	27.78	76.04	69.84	122	39.68
RF-Solver [34] (ICML 2025)	10.40	66.76	80.99	66.76	112	44.86
FireFlow [7] (ICML 2025)	7.16	70.17	80.86	68.44	18	7.47
ReInversion (Ours)	5.01	80.25	84.09	83.50	18	9.17
ReInversion* (Ours)	4.90	80.12	83.60	83.55	14	7.09

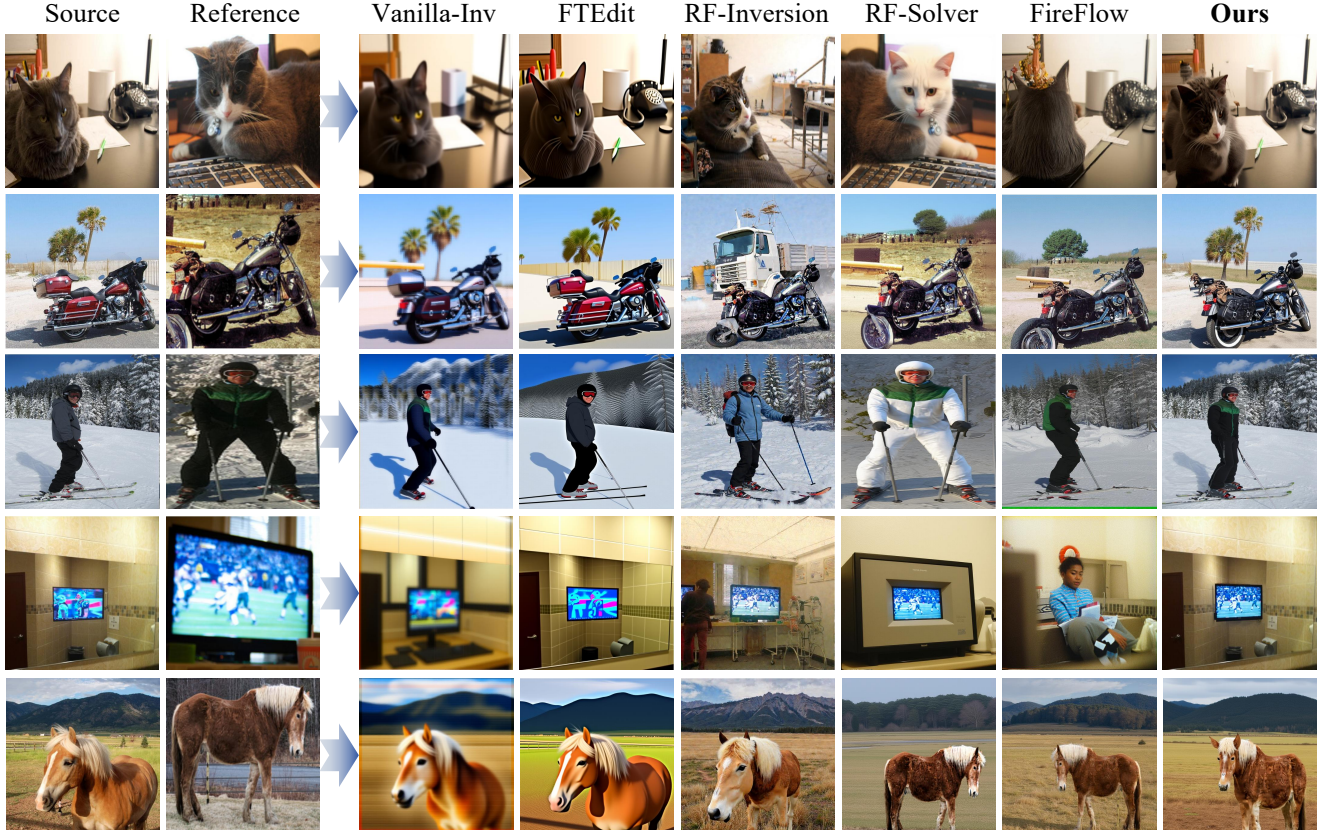


Figure 4. Qualitative comparisons with SOTA inversion-based methods. Our ReInversion (the last column) demonstrates superior performance compared to existing flow-based inversion methods.

and obscure the true performance of editing models. To ensure fairness and consistency, we manually filter these problematic samples and construct a curated subset containing 2,079 high-quality cases with clear and identifiable appearance cues, which we denote as COCOEE[†].

Evaluation Metrics. Our goal is to conduct EIE that faithfully transfers visual characteristics from the reference exemplar while preserving background and overall scene consistency of the source image, and achieves efficient inference. Accordingly, we adopt several complementary metrics in terms of quality, consistency, and efficiency. For quality, we measure the overall realism of the generated im-

ages using FID and Quality Score (QS). FID evaluates the distributional similarity between generated and real images, capturing global realism, while QS measures how well generated samples align with the distribution of real images. For consistency, we assess adherence to the reference exemplar and the source image, using CLIP-FG for foreground semantic consistency with the exemplar image and CLIP-BG for background preservation from the source image. For efficiency, we report the number of function evaluations (NFEs) and the inference time per test case.

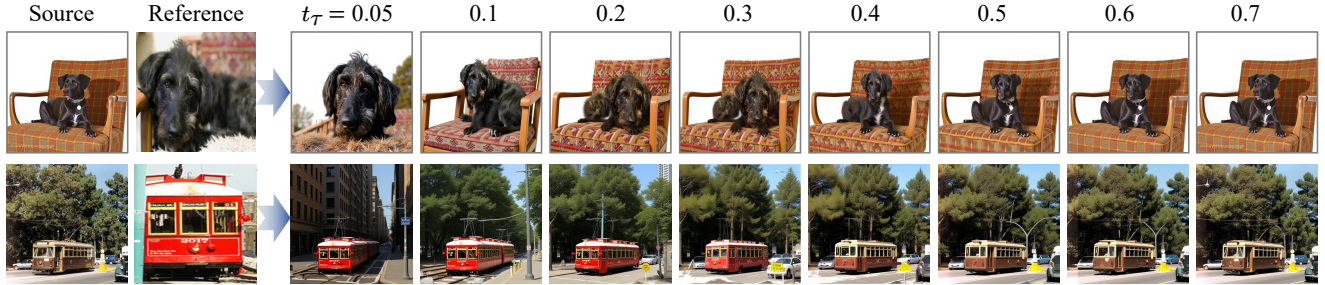


Figure 5. Ablation study on the effect of the hyperparameter t_τ .

5.2. Comparisons with SOTA Methods

We conduct both quantitative and qualitative experiments to evaluate the EIE performance of our method and compare it with state-of-the-art flow-based inversion methods. Specifically, we compare with Vanilla Inversion, FTEDIT [41], RF-Solver [34], FireFlow [7] and RF-Inversion [28]. All methods are re-implemented by us and evaluated using their optimal configurations.

Quantitative Comparisons We conduct a quantitative comparison between inversion-based methods and our proposed ReInversion, as summarized in Tab. 1. The results clearly demonstrate that our method achieves state-of-the-art performance across three key aspects: Quality, Consistency, and Efficiency. **(a) Quality.** The best existing method attains an FID of 7.16 and a QS of 70.17, whereas ReInversion achieves significantly better scores of 5.01 and 80.25 (and 4.90 and 80.12 under the deterministic velocity setting), indicating a marked improvement in generation fidelity and a closer match to the real image distribution. **(b) Consistency.** ReInversion exhibits superior foreground controllability and background coherence, achieving CLIP-FG and CLIP-BG scores of 84.09 and 83.50, respectively—outperforming the previous best results of 80.86 and 69.84. These results confirm that the proposed editing flow effectively merges reference and source content while maintaining spatial consistency across regions. **(c) Efficiency.** ReInversion requires only 18 NFEs and an average inference time of 9.17 seconds, substantially reducing computational cost compared to prior methods. The deterministic variant, ReInversion*, further decreases the cost to 14 NFEs and 7.09 seconds with nearly identical visual quality. Overall, ReInversion achieves an optimal balance between quality, controllability, and efficiency, establishing a new state of the art for training-free exemplar-guided image editing. More results in Supp. A.

Qualitative Comparisons As illustrated in Fig. 4, we provide a qualitative comparison of our proposed method against several state-of-the-art (SOTA) inversion-based techniques for visual fidelity and content preservation. The results span diverse scenarios, including street scenes, com-

Table 2. Effectiveness of the devised Mask-Guided Selective Denoising (MSD) strategy.

Name	CLIP-FG \uparrow	CLIP-BG \uparrow
ReInversion	81.80	68.96
+ MSD	84.09	83.50

plex animal textures, indoor settings, and outdoor landscapes. The results show that competitor methods frequently exhibit artifacts, color shifts, or structural degradation. These shortcomings are particularly apparent in their difficulty preserving fine details, such as the color of the cat’s mouth. A crucial advantage of our approach is its remarkably high fidelity in background preservation. For instance, in the tram and motorcycle scenes, competitor methods often introduce noticeable distortions or blurring in the surrounding environment. In contrast, our method maintains the integrity and fine detail of the background elements, such as the trees and buildings, with high consistency. Overall, our method consistently yields results that more faithfully adhere to both the style and content of the source image while maintaining superior visual quality, thereby demonstrating faithful exemplar-guided editing compared to the current SOTA inversion methods.

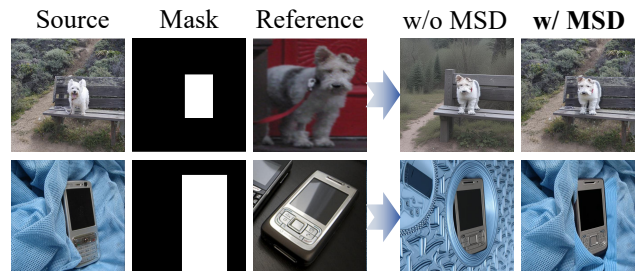


Figure 6. Qualitative analysis on Mask-Guided Selective Denoising. The red bounding boxes indicate the mask bounding box. MSD effectively preserves the background.

5.3. Ablation Study

We conduct ablation studies to illustrate the effectiveness of ReInversion and Mask-Guided Selective Denoising. These ablation studies are mainly based on 18 steps results of Flux-Kontext.

Effect of t_τ . The transition timestep t_τ is a crucial hyperparameter in our method, which governs the balance between preserving the source content and adopting the reference style. Specifically, the diffusion process is guided towards the *source* image content for time steps $t \in [0, t_\tau]$, and transitions to *reference* image guidance for $t \in [t_\tau, 1]$. As shown in Fig. 5, a small t_τ like 0.05 triggers an early switch to reference guidance, resulting in poor preservation of source structure and producing results closer to pure reconstruction than actual editing. Conversely, setting t_τ too large (e.g., $t_\tau \geq 0.5$) causes the model to follow the source guidance for too long. The structure becomes too rigid, making it hard for the reference to introduce modifications, and thus the final edits are barely noticeable. Based on this analysis, the most appropriate setting for t_τ lies within the range of $[0.1, 0.3]$, which offers a good balance between source preservation and editing flexibility.

Effectiveness of MSD. We first evaluate the effectiveness of the proposed mask-guided selective denoising (MSD) module. As shown in Fig. 6, introducing MSD significantly improves background preservation. The background in non-edited regions remains almost unchanged, while the version without mask often modifies these areas unintentionally. This improvement is further supported by the CLIP-BG score shown in Tab. 2, which increases from 68.96 to 83.50. In addition, the CLIP-FG score rises from 81.80 to 84.09, indicating that MSD not only protects the background but also enhances foreground alignment with reference. We attribute this to its ability to confine the editing operation within the target regions defined by the mask, preventing unintended modifications on irrelevant areas.

Table 3. Validation of the reformulation. ReInversion attains comparable editing performance to the Recon-Inv with only half the denoising steps, confirming the validity of the reformulation under negligible reconstruction error.

Method	CLIP-FG \uparrow	NFEs \downarrow	Time Cost \downarrow	Speedup
Recon-Inv	82.10	36	16.66s	1.0 \times
ReInversion	81.80	18	9.17s	1.82 \times

Validation of the Reformulation. While Sec. 4.2 provides a theoretical justification for reformulating Recon-Inv into ReInversion, their difference in practical EIE performance remains unknown. To further verify the validation of this reformulation, we compare the two implementations in Tab. 3, excluding the MSD module to focus on the effect of the reformulation. The results show that ReInversion

achieves quite close CLIP-FG score to the original Recon-Inv, confirming that the reformulation introduces no observable degradation in editing quality. Meanwhile, ReInversion reduces the NFEs by half and cuts the time cost per testing case by 45%, achieving a 1.82 \times speedup. This consistency and efficiency jointly validate our theoretical claim that Recon-Inv can be safely reformulated into the forward-only ReInversion process.

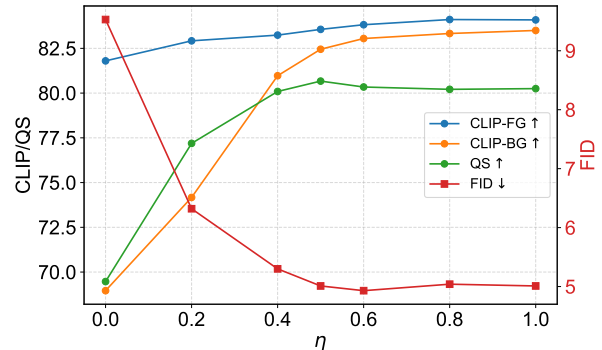


Figure 7. Ablation study on the effect of η .

Effect of η We further investigate the impact of the balancing coefficient η of Eq. 14, which controls the relative contribution of the deterministic velocity field v^* . As shown in Fig. 7, increasing η consistently improves all evaluation metrics—CLIP-FG, CLIP-BG, and QS rise while FID decreases—indicating enhanced visual fidelity and semantic consistency. This trend can be attributed to the stronger reconstruction guidance provided by a larger η , which helps preserve the structural integrity of the source while maintaining effective reference-driven modification. The performance stabilizes when η lies in the range of $[0.8, 1.0]$, demonstrating that the proposed MSD effectively achieves spatially selective denoising and enables adaptive balance between reconstruction and reference-guided editing.

6. Conclusion

In this work, we present ReInversion, a training-free framework for effective and efficient exemplar-guided image editing (EIE). First, we introduce Reconstruction-Based Inversion (Recon-Inv) to mitigate the noise drifts. Second, we reformulate Recon-Inv into ReInversion, enabling high-quality EIE within only 1 \times NFEs. Finally, we design Mask-Guided Selective Denoising (MSD) to preserve structural and color consistency in unedited regions. Extensive experiments demonstrate that ReInversion achieves superior quality, consistency, and efficiency. Our work suggests that training-free methods can achieve high-quality and efficient EIE, and we hope it can provide inspiration for future research in related fields.

References

- [1] Michael S. Albergo and Eric Vanden-Eijnden. Building normalizing flows with stochastic interpolants. In *Eleventh International Conference on Learning Representations*, 2023. 2
- [2] Tim Brooks, Aleksander Holynski, and Alexei A. Efros. Instructpix2pix: Learning to follow image editing instructions. In *Proceedings of the IEEE/CVF Conference on Computer Vision and Pattern Recognition*, pages 18392–18402, 2023. 2
- [3] Xi Chen, Lianghua Huang, Yu Liu, Yujun Shen, Deli Zhao, and Hengshuang Zhao. Anydoor: Zero-shot object-level image customization. In *Proceedings of the IEEE/CVF Conference on Computer Vision and Pattern Recognition*, pages 6593–6602, 2024. 1, 2, 13
- [4] Xi Chen, Zhifei Zhang, He Zhang, Yuqian Zhou, Soo Ye Kim, Qing Liu, Yijun Li, Jianming Zhang, Nanxuan Zhao, Yilin Wang, Hui Ding, Zhe L. Lin, and Hengshuang Zhao. Unireal: Universal image generation and editing via learning real-world dynamics. In *Proceedings of the IEEE/CVF Conference on Computer Vision and Pattern Recognition*, pages 12501–12511, 2025. 2
- [5] Guillaume Couairon, Jakob Verbeek, Holger Schwenk, and Matthieu Cord. Diffedit: Diffusion-based semantic image editing with mask guidance. In *Eleventh International Conference on Learning Representations*, 2023. 4
- [6] Chaorui Deng, Deyao Zhu, Kunchang Li, Chenhui Gou, Feng Li, Zeyu Wang, Shu Zhong, Weihao Yu, Xiaonan Nie, Ziang Song, Shi Guang, and Haoqi Fan. Emerging properties in unified multimodal pretrainings. *ArXiv*, abs/2505.14683, 2025. 2
- [7] Yingying Deng, Xiangyu He, Changwang Mei, Peisong Wang, and Fan Tang. Fireflow: Fast inversion of rectified flow for image semantic editing. In *Forty-second International Conference on Machine Learning*, 2025. 2, 3, 6, 7
- [8] Patrick Esser, Sumith Kulal, A. Blattmann, Rahim Entezari, Jonas Muller, Harry Saini, Yam Levi, Dominik Lorenz, Axel Sauer, Frederic Boesel, Dustin Podell, Tim Dockhorn, Zion English, Kyle Lacey, Alex Goodwin, Yannik Marek, and Robin Rombach. Scaling rectified flow transformers for high-resolution image synthesis. *ArXiv*, abs/2403.03206, 2024. 2
- [9] Daniel Garibi, Or Patashnik, Andrey Voynov, Hadar Averbuch-Elor, and Daniel Cohen-Or. Renoise: Real image inversion through iterative noising. In *European Conference on Computer Vision*, pages 395–413, 2024. 2, 3
- [10] Zhengyang Geng, Mingyang Deng, Xingjian Bai, J. Zico Kolter, and Kaiming He. Mean flows for one-step generative modeling. In *Advances in Neural Information Processing Systems*, 2025. 2
- [11] Ian J. Goodfellow, Jean Pouget-Abadie, Mehdi Mirza, Bing Xu, David Warde-Farley, Sherjil Ozair, Aaron C. Courville, and Yoshua Bengio. Generative adversarial nets. In *Advances in Neural Information Processing Systems*, pages 2672–2680, 2014. 2
- [12] Jiaqi Guo, Lianli Gao, Junchen Zhu, Jiabin Zhang, Siyang Li, and Jingkuan Song. Magicvfx: Visual effects synthesis in just minutes. In *Proceedings of the 32nd ACM International Conference on Multimedia*, 2024. 2
- [13] Jonathan Ho, Ajay Jain, and Pieter Abbeel. Denoising diffusion probabilistic models. In *Advances in Neural Information Processing Systems*, pages 6840–6851, 2020. 2
- [14] Tero Karras, Samuli Laine, and Timo Aila. A style-based generator architecture for generative adversarial networks. In *Proceedings of the IEEE/CVF Conference on Computer Vision and Pattern Recognition*, pages 4396–4405, 2019. 2
- [15] Tero Karras, Samuli Laine, Miika Aittala, Janne Hellsten, Jaakko Lehtinen, and Timo Aila. Analyzing and improving the image quality of stylegan. In *Proceedings of the IEEE/CVF Conference on Computer Vision and Pattern Recognition*, pages 8107–8116, 2020. 2
- [16] Tero Karras, Miika Aittala, Timo Aila, and Samuli Laine. Elucidating the design space of diffusion-based generative models. In *Advances in Neural Information Processing Systems*, pages 26565–26577, 2022. 2
- [17] Black Forest Labs, Stephen Batifol, Andreas Blattmann, Frederic Boesel, Saksham Consul, Cyril Diagne, Tim Dockhorn, Jack English, Zion English, Patrick Esser, Sumith Kulal, Kyle Lacey, Yam Levi, Cheng Li, Dominik Lorenz, Jonas Müller, Dustin Podell, Robin Rombach, Harry Saini, Axel Sauer, and Luke Smith. Flux.1 kontext: Flow matching for in-context image generation and editing in latent space. *ArXiv*, abs/2506.15742, 2025. 4, 5, 12
- [18] Yaron Lipman, Ricky T. Q. Chen, Heli Ben-Hamu, Maximilian Nickel, and Matt Le. Flow matching for generative modeling. In *Eleventh International Conference on Learning Representations*, 2023. 2
- [19] Gongye Liu, Haoze Sun, Jiayi Li, Fei Yin, and Yujiu Yang. Accelerating diffusion models for inverse problems through shortcut sampling. In *Proceedings of the Thirty-Third International Joint Conference on Artificial Intelligence*, pages 1101–1109, 2024. 4
- [20] Xingchao Liu, Chengyue Gong, and Qiang Liu. Flow straight and fast: Learning to generate and transfer data with rectified flow. In *Eleventh International Conference on Learning Representations*, 2023. 2
- [21] Haoguang Lu, Jiacheng Chen, Zhenguo Yang, Aurele Thokantche Gnanha, Fu Lee Wang, Qing Li, and Xudong Mao. Pairedit: Learning semantic variations for exemplar-based image editing. *ArXiv*, abs/2506.07992, 2025. 2
- [22] Chenlin Meng, Yutong He, Yang Song, Jiaming Song, Jiajun Wu, Jun-Yan Zhu, and Stefano Ermon. Sdedit: Guided image synthesis and editing with stochastic differential equations. In *Tenth International Conference on Learning Representations*, 2022. 2, 4
- [23] Ron Mokady, Amir Hertz, Kfir Aberman, Yael Pritch, and Daniel Cohen-Or. Null-text inversion for editing real images using guided diffusion models. In *Proceedings of the IEEE/CVF conference on computer vision and pattern recognition*, pages 6038–6047, 2023. 2
- [24] Chong Mou, Xintao Wang, Liangbin Xie, Jing Zhang, Zhongqiang Qi, Ying Shan, and Xiaohu Qie. T2i-adapter: Learning adapters to dig out more controllable ability for text-to-image diffusion models. In *Proceedings of the AAAI Conference on Artificial Intelligence*, pages 4296–4304, 2024. 2

- [25] Zhihong Pan, Riccardo Gherardi, Xiufeng Xie, and Stephen Huang. Effective real image editing with accelerated iterative diffusion inversion. In *Proceedings of the IEEE/CVF International Conference on Computer Vision*, pages 15866–15875, 2023. 2
- [26] Gaurav Parmar, Yijun Li, Jingwan Lu, Richard Zhang, Jun-Yan Zhu, and Krishna Kumar Singh. Spatially-adaptive multilayer selection for gan inversion and editing. In *Proceedings of the IEEE/CVF Conference on Computer Vision and Pattern Recognition*, pages 11389–11399, 2022. 2
- [27] William S. Peebles and Saining Xie. Scalable diffusion models with transformers. In *Proceedings of the IEEE/CVF International Conference on Computer Vision*, pages 4172–4182, 2023. 2
- [28] Litu Rout, Yujia Chen, Nataniel Ruiz, Constantine Caramanis, Sanjay Shakkottai, and Wen-Sheng Chu. Semantic image inversion and editing using rectified stochastic differential equations. In *Thirteenth International Conference on Learning Representations*, 2025. 2, 6, 7
- [29] Jiaming Song, Chenlin Meng, and Stefano Ermon. Denoising diffusion implicit models. In *Ninth International Conference on Learning Representations*, 2021. 2
- [30] Yang Song and Stefano Ermon. Generative modeling by estimating gradients of the data distribution. In *Advances in Neural Information Processing Systems*, pages 11895–11907, 2019. 2
- [31] Yang Song, Jascha Sohl-Dickstein, Diederik P. Kingma, Abhishek Kumar, Stefano Ermon, and Ben Poole. Score-based generative modeling through stochastic differential equations. In *Ninth International Conference on Learning Representations*, 2021. 2
- [32] Ashutosh Srivastava, Tarun Ram Menta, Abhinav Java, Avadhoot Jadhav, Silky Singh, Sargan Jandial, and Balaji Krishnamurthy. Reedit: Multimodal exemplar-based image editing. In *Proceedings of the IEEE/CVF Winter Conference on Applications of Computer Vision*, pages 929–939, 2025. 2
- [33] Bram Wallace, Akash Gokul, and Nikhil Vijay Naik. Edict: Exact diffusion inversion via coupled transformations. In *Proceedings of the IEEE/CVF Conference on Computer Vision and Pattern Recognition*, pages 22532–22541, 2023. 2
- [34] Jiangshan Wang, Junfu Pu, Zhongang Qi, Jiayi Guo, Yue Ma, Nisha Huang, Yuxin Chen, Xiu Li, and Ying Shan. Taming rectified flow for inversion and editing. In *Forty-second International Conference on Machine Learning*, 2025. 3, 6, 7
- [35] Chenfei Wu, Jiahao Li, Jingren Zhou, Junyang Lin, Kaiyuan Gao, Kun Yan, Sheng ming Yin, Shuai Bai, Xiao Xu, Yilei Chen, Yuxiang Chen, Zecheng Tang, Zekai Zhang, Zhengyi Wang, An Yang, Bowen Yu, Chen Cheng, Dayiheng Liu, Deqing Li, Hang Zhang, Hao Meng, Hu Wei, Jingyuan Ni, Kai Chen, Kuan Cao, Liang Peng, Lin Qu, Minggang Wu, Peng Wang, Shuting Yu, Tingkun Wen, Wensen Feng, Xiaoxiao Xu, Yi Wang, Yichang Zhang, Yongqiang Zhu, Yujia Wu, Yuxuan Cai, and Zenan Liu. Qwen-image technical report. *ArXiv*, abs/2508.02324, 2025. 12
- [36] Chenyuan Wu, Pengfei Zheng, Ruiran Yan, Shitao Xiao, Xin Luo, Yueze Wang, Wanli Li, Xiyan Jiang, Yexin Liu, Junjie Zhou, Ze Liu, Ziyi Xia, Chaofan Li, Haoge Deng, Jiahao Wang, Kun Luo, Bo Zhang, Defu Lian, Xinlong Wang, Zhongyuan Wang, Tiejun Huang, and Zheng Liu. Omnigen2: Exploration to advanced multimodal generation. *ArXiv*, abs/2506.18871, 2025. 1
- [37] Shaojin Wu, Mengqi Huang, Wenxu Wu, Yufeng Cheng, Fei Ding, and Qian He. Less-to-more generalization: Unlocking more controllability by in-context generation. In *Proceedings of the IEEE/CVF International Conference on Computer Vision*, pages 18682–18692, 2025. 2, 13
- [38] Weihao Xia, Yulun Zhang, Yujiu Yang, Jing-Hao Xue, Bolei Zhou, and Ming-Hsuan Yang. Gan inversion: A survey. *IEEE Transactions on Pattern Analysis and Machine Intelligence*, 45:3121–3138, 2021. 2
- [39] Shitao Xiao, Yueze Wang, Junjie Zhou, Huaying Yuan, Xingrun Xing, Ruiran Yan, Shuting Wang, Tiejun Huang, and Zheng Liu. Omnigen: Unified image generation. In *Proceedings of the IEEE/CVF Conference on Computer Vision and Pattern Recognition*, pages 13294–13304, 2025. 1, 2
- [40] Chenxi Xie, Ming hui Li, Shuai Li, Yuhui Wu, Qiaosi Yi, and Lei Zhang. Dnaedit: Direct noise alignment for text-guided rectified flow editing. In *Advances in Neural Information Processing Systems*, 2025. 2, 3
- [41] Pengcheng Xu, Boyuan Jiang, Xiaobin Hu, Donghao Luo, Qingdong He, Jiangning Zhang, Chengjie Wang, Yunsheng Wu, Charles Ling, and Boyu Wang. Unveil inversion and invariance in flow transformer for versatile image editing. In *Proceedings of the IEEE/CVF Conference on Computer Vision and Pattern Recognition*, pages 28479–28489, 2025. 2, 3, 6, 7
- [42] ya sheng sun, Yifan Yang, Houwen Peng, Yifei Shen, Yuqing Yang, Han Hu, Lili Qiu, and Hideki Koike. Imagebrush: Learning visual in-context instructions for exemplar-based image manipulation. In *Advances in Neural Information Processing Systems*, pages 48723–48743, 2023. 1, 2
- [43] Binxin Yang, Shuyang Gu, Bo Zhang, Ting Zhang, Xuejin Chen, Xiaoyan Sun, Dong Chen, and Fang Wen. Paint by example: Exemplar-based image editing with diffusion models. In *Proceedings of the IEEE/CVF Conference on Computer Vision and Pattern Recognition*, pages 18381–18391, 2023. 1, 2, 5, 13, 14
- [44] Ahmet Burak Yildirim, Hamza Pehlivan, Bahri Batuhan Bilecen, and Aysegul Dundar. Diverse inpainting and editing with gan inversion. In *Proceedings of the IEEE/CVF International Conference on Computer Vision*, pages 23063–23073, 2023. 2
- [45] Lvmin Zhang, Anyi Rao, and Maneesh Agrawala. Adding conditional control to text-to-image diffusion models. In *Proceedings of the IEEE/CVF International Conference on Computer Vision*, pages 3836–3847, 2023. 2
- [46] Jiapeng Zhu, Yujun Shen, Deli Zhao, and Bolei Zhou. In-domain gan inversion for real image editing. In *European Conference on Computer Vision*, pages 592–608, 2020. 2

Reversible Inversion for Training-Free Exemplar-guided Image Editing

Supplementary Material

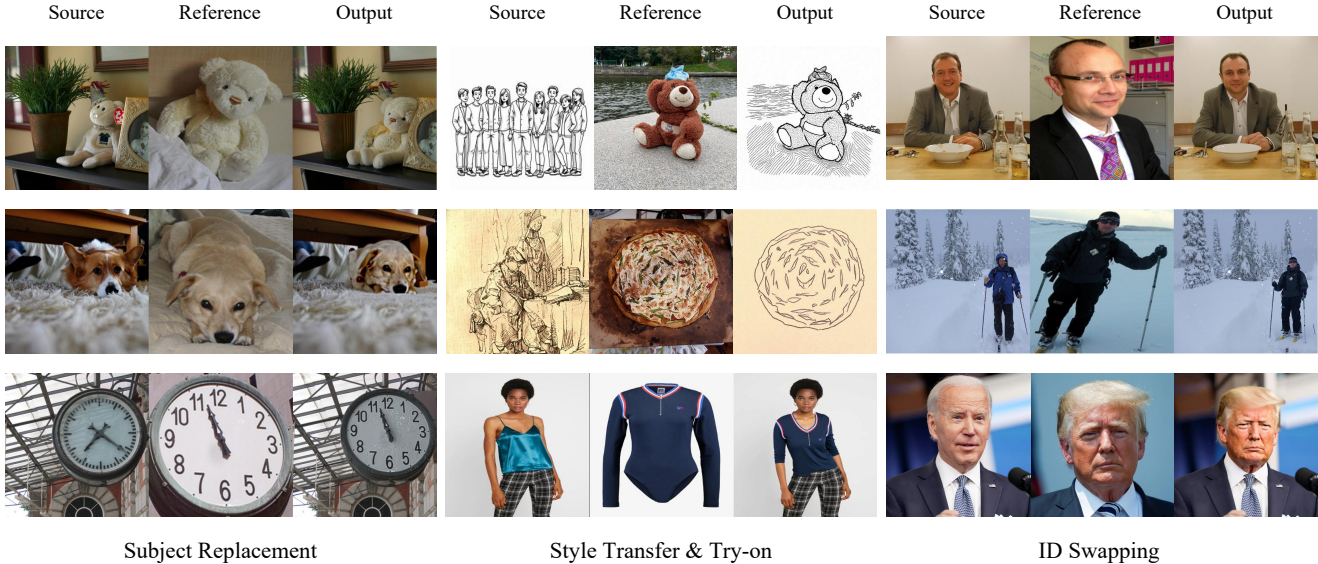


Figure H. Additional results of ReInversion across three main categories: Subject Replacement (left), Style Transfer & Try-on (center), and ID Swapping (right). Each triplet of images shows the Source image, the Reference image (providing the target subject/content/ID), and the final Output generated by the model.

A. Additional Results and Analysis

To provide a comprehensive evaluation of the ReInversion methodology, we present additional results across a spectrum of challenging image manipulation tasks, as detailed in Fig. H. These results underscore the versatility and precise control afforded by our method, which is broadly categorized into Subject Replacement, Style Transfer & Try-on, and ID Swapping.

Subject Replacement. The capability for effective Subject Replacement is demonstrated by the model’s proficiency in substituting a targeted entity within a source image with a new subject derived from a reference image, all while meticulously preserving the background and surrounding context. For instance, the top and middle rows of the left section illustrate the seamless integration of new subjects—specifically, stuffed animals and dogs—into novel environments. Furthermore, the bottom example showcases fine-grained content editing, where the numeric display on the clocks is accurately altered, proving the method’s robustness across diverse object types.

Style Transfer and Visual Try-on. This application highlights the method’s ability to disentangle content from style and precisely map features from a reference image onto a source image. The central column of Fig. H provides compelling evidence. We successfully execute style trans-

fer, converting photographic content into different artistic domains, as seen in the conversion of the teddy bear photograph into a sketch-like output (top-center). Crucially, the bottom example demonstrates high-fidelity garment try-on. The specific clothing style from the reference image is accurately transferred and rendered onto the source subject, conforming correctly to the subject’s pose, lighting, and geometric structure.

Identity (ID) Swapping. The ID Swapping task represents a stringent test of the model’s ability to manipulate semantic information while maintaining structural consistency. Our method successfully replaces the identity of the person in the source image with the identity provided by the reference image. This is accomplished while rigorously preserving the original facial expression, head pose, and background details. The results in the rightmost column, including the challenging example of swapping the identities of well-known public figures (bottom-right), provide clear validation that ReInversion achieves precise ID manipulation with exceptional photographic realism and identity coherence.

In summary, the results presented in Fig. H affirm that ReInversion is a robust and highly controllable image synthesis framework capable of managing complex, multi-faceted image editing requirements with high fidelity.

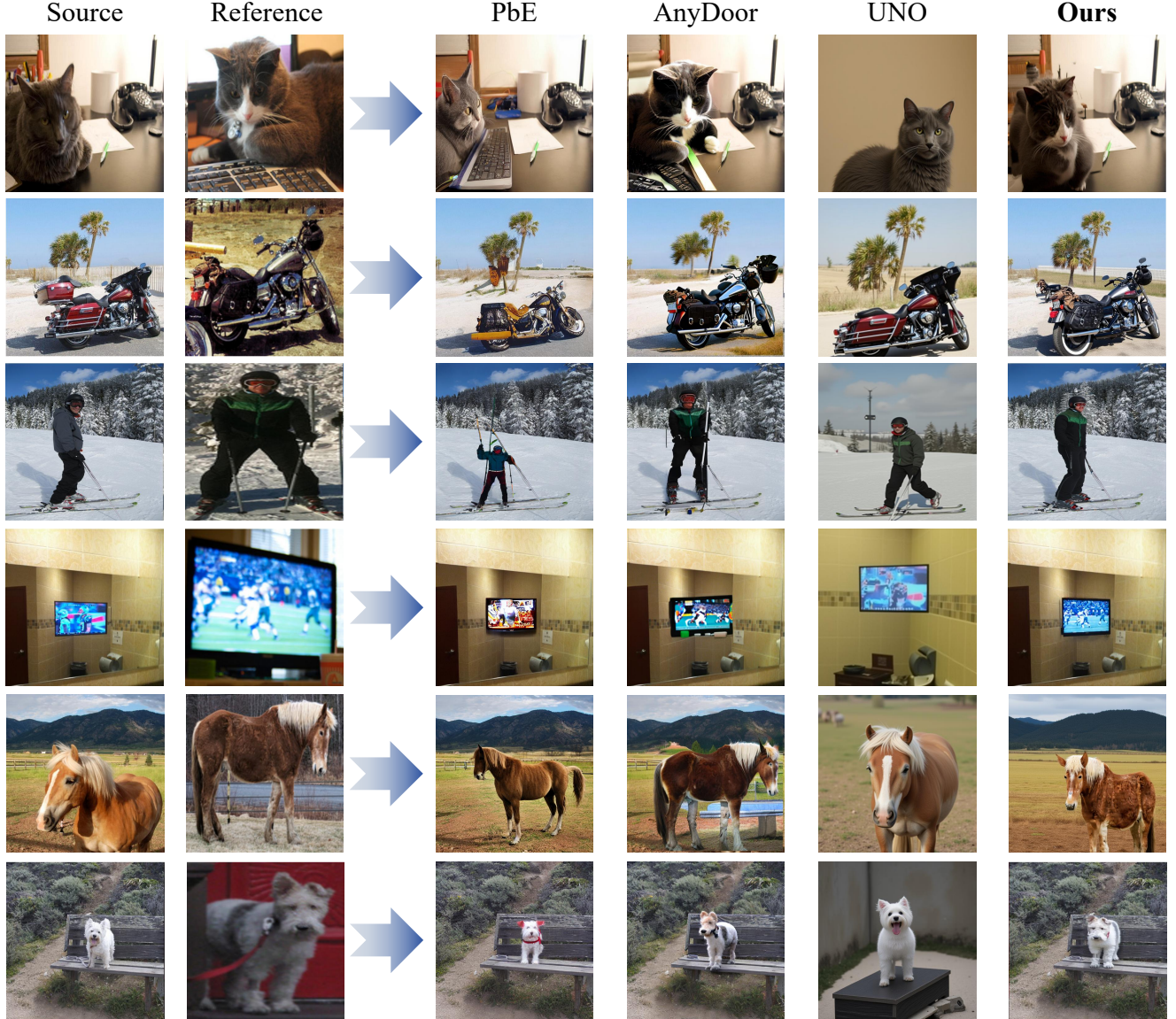


Figure I. Qualitative comparisons with pre-trained models.

B. Additional Backbone and Inference Steps

To assess the generality of our approach, we further evaluate ReInversion on two distinct EIE backbones, Qwen-Image-Edit and Flux-Kontext, under multiple inference steps (8/18/28 NFEs). In detail, we quantize the DiT and text encoder of Qwen using 4-bit NF4 quantization to reduce memory footprints and support efficient inference. The results are summarized in Tab. D.

Transferability to New Backbones. ReInversion consistently improves or maintains editing quality across both architectures, demonstrating that our formulation is not tied to a particular model design. In both Qwen and Kontext, increasing the guidance steps steadily improves FID, QS,

Arch	FID↓	QS↑	CLIP-FG↑	CLIP-BG↑	NFEs↓
Qwen	4.88	78.06	72.56	83.83	8
Qwen	4.84	76.15	72.47	83.76	18
Qwen	4.65	78.20	82.30	83.97	28
Kontext	5.12	78.63	83.03	83.43	8
Kontext	5.01	80.25	84.09	83.50	18
Kontext	5.05	80.73	84.68	83.51	28

Table D. Quantitative results on different backbones (Qwen-Image-Edit [35] and Flux-Kontext [17]) and inference steps (8, 18, 28) of our ReInversion on COCOEE[†].

and foreground alignment, confirming that our method can be seamlessly adopted by heterogeneous transformer-based


```

1 # Inputs: X_src, X_ref, Mask, t_tau, eta
2
3 X = torch.randn_like(X_src)
4
5 for t in (timesteps):
6     if t < t_tau: # stage 1
7         v_theta = model(X, t, X_src) # conditioned on source image
8
9         # update X
10        X = X + v_theta * delta_t
11    else: # stage 2
12        v_theta = model(X, t, X_ref) # conditioned on reference image
13        v = (X_src - X) / (1 - t) # deterministic velocity
14
15        # update X (MSD)
16        X[Mask==0] += (v[Mask==0] * eta + v_theta[Mask==0] * (1 - eta)) * delta_t # background
17        X[Mask==1] += v_theta[Mask==1] * delta_t # foreground
18 return X

```

Figure J. Python-style pseudo-code of the proposed ReInversion.

editors.

Efficient EIE on Flux-Kontext. On Kontext, ReInversion achieves strong editing performance even under very small NFEs. Notably, 8-step and 18-step generations already match or exceed the quality of longer runs: QS increases from 78.63→80.25 and CLIP-FG improves from 83.03→84.09 when moving from 8 to 18 steps, with diminishing returns at 28 steps. This indicates that Kontext’s architecture synergizes well with our reformulation, enabling high-quality, low-cost EIE.

Short-step Behavior on Qwen-Image-Edit. In contrast, the 8-step and 18-step results on Qwen show weaker CLIP-FG performance (≈ 72.5) compared to its longer 28-step setting. We attribute this to Qwen’s design: it is not distilled for low-NFE inference and lacks explicit consistency-oriented constraints. Its default inference schedule uses 50 steps, and the model has not been optimized for short-trajectory decoding. Consequently, aggressive step reduction leads to noticeable degradation in reconstruction fidelity and semantic consistency, which our method cannot fully compensate for.

Overall, these findings show that ReInversion not only generalizes across backbones but can also unlock fast editing regimes for models that are structurally compatible, while exposing limitations in architectures that depend on long diffusion trajectories.

C. Comparisons with Pre-trained Models

We compared our approach against three established pre-trained EIE models: PbE [43], AnyDoor [3], and UNO [37]. As shown in Fig. 1, the pre-trained models exhibit significant shortcomings across various editing tasks. Specifically,

UNO struggles with background preservation, often introduces severe distortion or entirely replacing source scene elements, as seen in the first (cat) and third (skier) rows. The PbE model frequently generates results with a stylistic inconsistency, where the aesthetic quality or ‘painting style’ of the edited subject mismatches that of the source and reference images (e.g., the distinct style of the cat and the skier). AnyDoor performs marginally better in maintaining background structure but consistently struggles with accurately capturing and transferring the specific, fine-grained characteristics of the reference image, such as subtle textures and subject contours. In contrast, our proposed method effectively addresses these deficiencies. It delivers results that not only precisely transfer the reference appearance but also ensure high fidelity to the source image’s background and consistent visual style, resulting in more realistic and faithful image edits.

Moreover, it is worth acknowledging that pre-trained models (e.g., AnyDoor, PbE) exhibit superior stability in extreme editing scenarios. Benefiting from extensive exposure to large-scale datasets during training, these models possess a robust generative prior. Consequently, even when they fail to strictly follow the reference guidance, they tend to produce visually plausible outputs with realistic textures. In contrast, our training-free approach may encounter reduced realism when handling complex semantic transformations.

D. Python-style Pseudo-Code

As illustrated in Listing J, the procedure of ReInversion is straightforward and implementation-friendly. It performs a two-stage inversion process, first conditioned on the source

image and then guided by the reference image with a masked update. Despite its simplicity, this formulation efficiently achieves high-quality inversion while supporting flexible masked editing.

discriminately. By removing these bad cases, our evaluation on the curated subset provides a more accurate signal of the models’ actual editing capabilities.



Figure K. Low-quality reference images in COCOEE.

Arch	FID↓	QS↑	CLIP-FG↑	CLIP-BG↑	NFEs↓
RF-Inversion	9.13	56.84	74.40	64.60	56
FTEdit	23.25	23.75	73.49	69.10	122
RF-Solver	9.58	64.84	78.78	65.03	112
FireFlow	6.82	64.05	78.07	66.95	18
Ours (w/o MSD)	6.33	63.79	79.06	71.46	18
Ours (w/ MSD)	3.77	74.05	80.27	83.69	18

Table E. Quantitative results on original COCOEE.

E. Details on Evaluation Dataset

As mentioned in the main paper, COCOEE [43] contains a notable portion of ambiguous or incomplete samples that are unsuitable for EIE evaluation, as shown in Fig. K. We filter these low-quality images out of COCOEE and construct a curated subset of 2,079 samples (COCOEE[†]) from the original COCOEE dataset for quantitative evaluation.

To ensure that this selection is not biased, we also conduct experiments on the original COCOEE dataset (Tab. E). ReInversion still outperforms existing inversion approaches on the original COCOEE. It is important to note that this filtering is model-agnostic. The discarded samples pose challenges to both inversion-based and pre-trained methods in-